Research Article Vol. 4, No. 1 / 15 January 2021 / OSA Continuum 47

High harmonic generation in AlN due to out-of-surface electron orbitals

J. Seres,[1,*] E. Seres,[1] C. Serrat,[2] and T. Schumm[1]

[1]Atominstitut - E141, Technische Universität Wien, Stadionallee 2, 1020 Vienna, Austria
[2]Universitat Politècnica de Catalunya, Departament de Física, Colom 11, 08222 Terrassa, Spain
[*]jozsef.seres@tuwien.ac.at

Abstract: High harmonic generation in solids is commonly considered as a bulk process. However, there is a controversy whether the experimentally observed effects can in their entirety be described by a pure bulk model. Our results based on beam propagation and spectral characteristics provide a clear signature of the importance of surface effects on the origin of the harmonic generation in solids. Computations performed with a time-dependent density-functional approach corroborate the experimental measurements.

1. Introduction

High harmonic generation (HHG) in solids is an increasingly popular method and tool to produce coherent ultrashort pulses in the vacuum ultraviolet (VUV) or even beyond, in the extreme ultraviolet [1–5], and to study the high order nonlinear properties [6] and band structure of solids [1]. The underlying physics, however, is still not well understood. Recently, most accepted theories describe the generation of harmonics as bulk processes [7–10] governed by time dependent inter-band polarizations and intra-band electron currents. Surface effects are generally expected to make only a small contribution [11]. Several experiments, however, even the first observations of the phenomenon [12,13], pointed in the direction that the generated harmonics would have a surface origin [3,4,14–18].

In this study, we present experiments that contradict the bulk origin of HHG in solids and that can be explained by a surface origin. Additionally, our experiments reveal that the harmonics are generated outside (but in close vicinity) of the material surface due to out-of-surface electron orbitals. Measurements were made with different semiconductors like AlN, GaN, MgO and insulators like Al_2O_3, LiF, CaF_2 and MgF_2 and we found a similar behavior in all of them. In the present work, we report in particular the measurements for AlN, because its large damage threshold and large nonlinearity enabled experiments in the broadest parameter range. We observe exclusively collinear propagation of the driver laser's and the generated harmonics' beams for all angles of incident and observe only odd harmonics transmission. This contrasts with what would be expected from the 6mm (C_{6v}) crystal symmetry of the bulk crystal, which would also support the generation of even harmonics. Supposing however a 2D quasi-layer on the crystal surface formed by a conduction band wave function localized on the Al atoms of the surface, pointing out of the surface, (which implies 6/mmm (D_{6h}) symmetry) our model and calculations support the absence of even harmonics and the propagation characteristics are well explained.

2. Experimental setup

The measurement setup is shown in Fig. 1. It is based on a Ti:sapphire frequency comb (FC8004, Menlo Systems) with basic operation parameters of 0.9 W, 108 MHz repetition rate at 800 nm central wavelength. The spectral phase of the laser pulses was pre-set by chirped mirror-pairs and a wedge-pair to get dispersion-compensated 17 fs focused laser pulses on the AlN film. A lens with focal length of 10 mm focused the laser beam resulting in a beam waist of 5.5 ± 0.5 µm, an on-axis peak intensity of 1.0 ± 0.2 TW/cm^2 and a Rayleigh length of 120 ± 20 µm (in

#404942 https://doi.org/10.1364/OSAC.404942
Journal © 2021 Received 7 Aug 2020; accepted 9 Dec 2020; published 24 Dec 2020

OSA CONTINUUM

vacuum). AlN (0001) film, 30 nm thick, was grown [5] on a 100 μm thick sapphire substrate and was characterized by reflection high energy electron diffraction. The sample was placed on a rotation stage to perform measurements at different angles of incidence (AOI).

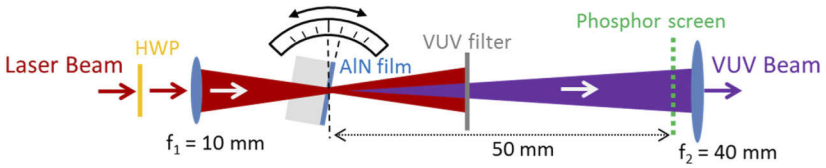

Fig. 1. Schematic showing the experimental arrangement for measuring solid HHG from AlN thin film. HWP: half-wave plate.

3. Beam propagation results

Figure 2(a) shows the spatial separation of harmonic orders that would be expected when the harmonics were generated inside an AlN medium (bulk HHG). The sapphire substrate does not play an important role, here because it is a plan-parallel plate and the harmonics generated inside the sapphire are orders of magnitude weaker than those from AlN [5]. The harmonics generated inside the medium (dashed lines) propagate collinearly with the laser beam (red line) until the rear surface of the AlN film. After refraction on the surface, they should propagate at different angles due to the different refractive indexes for the different colors ($n_{800} = 2.11$, $n_{267} = 2.37$, $n_{160} = 2.71$). On the Phosphor screen, situated 50 mm from the source, the beams should hence be observed at different positions. The expected relative positions of the 3rd and 5th harmonic beams to the laser beam is calculated in Fig. 2(b) using the measured susceptibility and refractive index of wurtzite AlN (w-AlN) [19–21]. For the 3rd harmonic, where data are available, the positions of both ordinary and extraordinary beams are provided. According to the calculations in Fig. 2(b), at 15° and 45° AOIs, the beam of the 3rd harmonic should be displaced by 1.24 (1.26) mm and 4.9 (5.3) mm, respectively, where the value of the extraordinary beam is in the parentheses. For 45° AOI especially, the displacement is well visible (the predicted beam positions are indicated in the figure) because it is much larger than the 2.9 mm radius (HWHM) of the laser beam.

A previous experiment [3], however, reported that the generated harmonics co-propagate with the laser beam for harmonics generated near the rear surface of a wedge-shaped sapphire medium. To address this contradiction with the "bulk model", we performed an experiment using the previously mentioned 30-nm-thick AlN film on a 100-μm-thick sapphire substrate, both with (0001) orientation. The AlN film was on the rear surface as it is shown in the experimental arrangement in Fig. 1, and the laser was also focused onto the rear surface. To observe the beam profiles of the 3rd harmonic at different AOIs, a VUV bandpass filter (266-BB-1D, Pelham Research Optical L.L.C.) transparent at the wavelength of the 3rd harmonic, was inserted to block the laser beam. The measured beam profile of the laser beam without the VUV filter and that of the 3rd harmonic with filter at two AOIs of 15° and 45° are presented in Fig. 2(c). Independently of the AOI, the measurements show no displacement of the 3rd harmonic beam within the measurement error (< 1 mm, originating from beam profile distortion of the laser beam due to the astigmatism in the substrate). At 45°, the harmonic beam is weaker due to the beam profile distortion of the tightly focused laser beam caused by the astigmatism in the substrate and the Fresnel reflection loss of the laser beam at the surfaces of the sapphire substrate.

OSA CONTINUUM

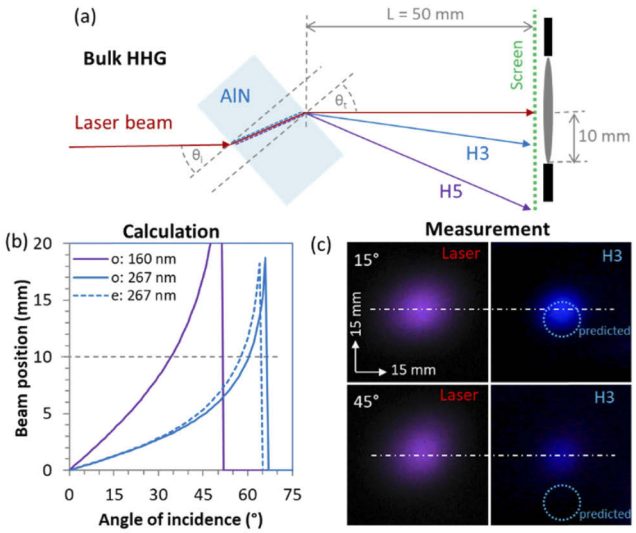

Fig. 2. (a) Expected angle-dependence for bulk HHG. The generated harmonic beams should propagate in different directions after leaving the generating medium of AlN (b) The calculated positions of the harmonic beams are strongly dependent on the AOI θ_i and blocked after exceeding the 10 mm radius of the lens (noted by grey dashed line). o: ordinary and e: extraordinary beams. (c) Instead, the measured beam profiles of the laser beam and the 3rd harmonic beam at AOIs of 15° and 45° measured on a phosphor screen placed at 50 mm from the AlN film does not exhibit the predicted change of direction (blue dotted circles).

4. Measurement of the harmonic spectra

It was not possible to perform the same beam profile measurement for the 5th harmonic beam because of its much lower intensity and conversion efficiency of about 10^{-8} compared to the stronger 3rd harmonic generated with about 10^{-4} efficiency. However, we were able to obtain results on the beam direction by means of another experiment. Removing the screen and the VUV filter, the spectra of the generated harmonics were measured at several AOIs up to 75°. A VUV-grade MgF_2 lens (Fig. 1) focused the generated 5th harmonic beam to the input slit of a VUV monochromator (McPherson 234/302) while at the same time the 3rd harmonic beam was near collimated. The spectrally resolved beam was detected with a VUV photomultiplier (Hamamatsu R6836), sensitive in the 115-320 nm spectral range. The HHG source and the VUV monochromator were in vacuum with a background pressure of 10^{-3} mbar to avoid the reabsorption of the 5th harmonic. We performed measurements at two arrangements, that is, having the AlN film on the front side and on the rear side of the substrate.

As can be seen in Fig. 2(b), the holder of the lens should block the 5th harmonic beam beyond 30° AOI (horizontal dashed line) and at 45° AOI, the 5th harmonic beam should be 18.7 mm away from the laser beam. Even for the 3rd harmonic, at angles larger than 55°, the beam should not pass the lens and could not reach the spectrograph. Additionally, at an AOI larger than 62° and 51° for the 3rd and 5th harmonics, respectively, beyond the angles of total reflection, we should not observe the harmonics at all.

However, as it can be seen in Fig. 3(a), both harmonics were observed at every measured AOIs up to the largest measured AOI of 75°, in the case that the AlN film was on the front surface. The intensity of 3rd harmonic showed only a weak dependence on the AOI. The intensity of the 5th harmonic decreased because of the longer propagation path through the AlN layer, which has

OSA CONTINUUM

some absorption at the wavelength of the 5th harmonic. A similar behavior was found when the AlN film was on the rear surface as can be seen in Fig. 3(b). In this case, the intensity of both harmonics decreased due to astigmatism caused by the substrate and the Fresnel reflection loss of the laser beam at the surfaces of the sapphire substrate. At 75° AOI, the 5th harmonic became too weak to be observable. In both cases, we still observed the harmonics at AOIs beyond the angle limits (55°, 30°) of the aperture predicted in Fig. 2(b) and even beyond the total reflection angles. Additionally, both harmonics behaved similarly with respect to hitting the detector. We are hence confident to conclude that the 5th harmonic, similarly to the 3rd harmonic, co-propagated with the laser beam.

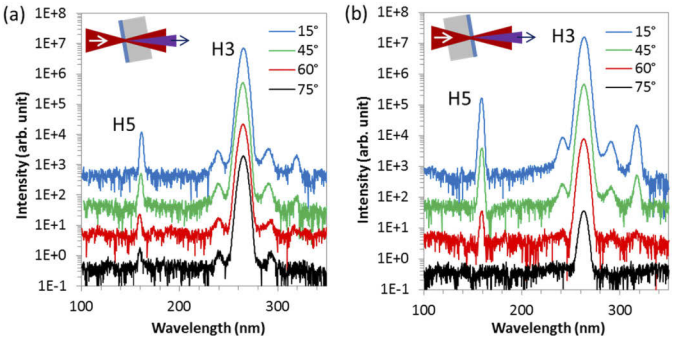

Fig. 3. Spectra of the generated harmonics were measured at different angles of incidence when the AlN film was on the (a) front surface or (b) rear surface of the substrate. The spectra are shifted vertically for better visibility. The insets show the arrangement, with the sapphire substrate depicted in gray and the AlN film in blue.

5. Comparation to numerical calculations

Beyond the appearance of the 5th harmonic at 160 nm and the 3rd harmonic at 267 nm, other spectral components were also produced as it can be seen in Fig. 3 and also in Fig. 4(a). The measurement shown in Fig. 4(a) is like Fig. 3(b) but at a small $\theta_i \approx 5°$ AOI, which is used to avoid back reflection of the focused laser beam into the oscillator. The measurements were made up to 600 nm. The small peaks at 240 nm and 290 nm originate from the fluorescence of the multi-photon excited AlN [22]. The peaks at 320 nm and 533 nm (5/2 and 3/2 harmonic orders) are the second diffraction order of the 5th and 3rd harmonics, an artifact of the VUV spectrometer. Even harmonics, 2nd, 4th and 6th at 400 nm, 200 nm and 133 nm, respectively, were not observed. The absence of the 2nd harmonic (not presented here) even at larger AOI differs from what is expected for bulk HHG. Bulk w-AlN is a 6mm (C_{6v}) crystal class, which involves 2nd harmonic generation for $\theta_i > 0°$ using the perturbative theory [23]. For the 4th and higher order harmonics, the susceptibility tensors of different crystal classes are not available. Therefore, we computed the harmonics spectra beyond the perturbative theory, using the full quantum time-dependent density-functional approach implemented in the first-principles code Octopus [24,25], which allows an accurate treatment of time-dependent electronic currents in complex molecular and extended systems. For the calculations, a Hartwigsen-Goedecker-Hutter LDA pseudopotential was used.

Calculations were made for bulk w-AlN, which is a commonly accepted way to compute HHG in solids. We adopt the w-AlN unit cell with a hexagonal close-packed structure of four basis atoms with the lattice parameters as described in [26] and highlighted by a dashed-line black frame in Fig. 5(a). Our bulk computations for the w-AlN crystal include 3D periodic boundary conditions, with a grid spacing of 20 pm and number of k-points in all three dimensions are $n_k = 6$

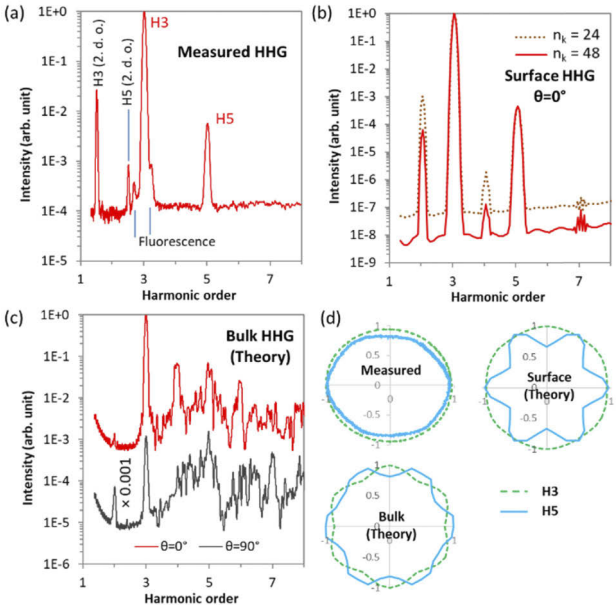

Fig. 4. Comparison of (a) the measured HHG spectrum to theoretical ones calculated for different scenarios. (d. o. = diffraction order). (b) Calculated harmonic spectrum assuming HHG on the surface at two number of k-points or (c) calculated harmonic spectra assuming bulk HHG for a w-AlN crystal at two angles of propagation θ. (d) Measured and calculated linear polarization dependences of H3 and H5.

to obtain converged results, and excitation in the out-of-plane direction. The harmonic spectrum

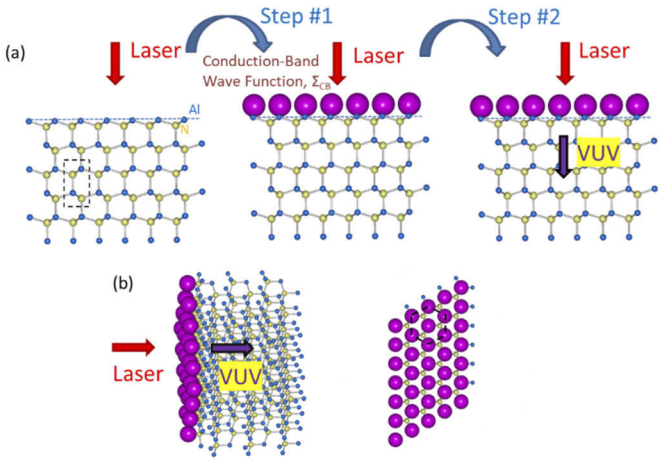

Fig. 5. (a) The process of HHG on w-AlN crystal structure (side view) with a laser beam reaching the front surface. Step #1: formation of the surface conduction band wave function Σ_{CB}., pointing out of the surface and forming a quasi 2D layer over the surface. The wave function is represented with violet spheres positioned at the Al atoms on the surface. Step #2: HHG from Σ_{CB}. (b) w-AlN 3D crystal structure near side view and top view show the hexagonal structure (highlighted by black dashed line) of the Σ_{CB} wave function.

OSA CONTINUUM

is computed from the Fourier transform of the time-derivative of the total electronic current as described in [10]. Figure 4(c) shows that, as expected from perturbative theory, the direction of propagation of $\theta = 0°$, the 2nd harmonic is not (or very weakly) generated, however the 4th and 6th harmonics should be present. At $\theta = 90°$, the 2nd harmonic appears but remains weak. Under phase matching condition, even such a weak 2nd harmonic can build up due to propagation and a w-AlN crystal can be used for 2nd harmonic generation [27]. In our measurements, however, we did not observe any sign of the 2nd, 4th and 6th harmonics, which provides an additional discrepancy of our experimental observations compared to the result expected from bulk HHG theory. Beyond the absence of even harmonics, the calculated spectrum differs in additional, qualitative features. The calculation in Fig. 4(c) predicts a broad and strongly structured spectral part beyond the 3rd harmonic, which is common for spectra calculated in bulk [8,10,18]. In the measurements, however such feature is not observed, and the calculated 5th harmonic is hardly distinguishable comparing to the measurements where it is well visible and clean.

6. Proposed surface model of solid HHG

To resolve this controversy also from a theoretical perspective, we look into the rearrangement of atoms at the AlN's surface and the surface wave functions at the edge of the valence and conduction bands (we name them as Σ_{VB} and Σ_{CB}, respectively for simpler reference). Such calculations were already made for Al_2O_3 [28] although similar behavior can be expected for AlN. Indeed, in both crystals, Σ_{CB} is composed by Al 3s orbitals [19,28] while Σ_{VB} is formed by the 2p orbitals of O or N and Al-O or Al-N bonding orbitals for Al_2O_3 or AlN, respectively.

In our case, compared to [28], the rearrangement of atoms on the surface alone cannot play an important role. Even if one assumed an arrangement with inversion symmetry at the surface with no production of even harmonics, hundreds of deeper layers within the phase-matching length would produce them and hence this would not explain the lack of even harmonics in the measurements. Therefore, for simplicity we present the crystal structure on the surface in Fig. 5 without that rearrangement. According to the calculations, Fig. 5 in [28], Σ_{CB} should have an important effect. This wave function is localized almost exclusively on the Al atoms of the surface and pointing out and it is situated outside of the surface, while the states of Σ_{VB} are localized in the surface layer and the sub-surface layer. In Fig. 5(b)–5(d), the surface wave function Σ_{CB} is represented by violet spheres. From our estimation, its localization outside of the crystal is the essential factor, not its exact shape.

In our understanding, the HHG in solids can be described with two steps as shown in Fig. 5(a). #1: in the strong laser field, the electrons move from the valence band into the conduction band by multi-photon or tunnel excitation; #2: high harmonics are generated from the states Σ_{CB} (depicted by purple spheres in Fig. 5) located just outside the crystal surface. According to this model, the generated harmonics propagate collinearly to the laser beam because outside of the crystal the refractive index can be considered as $n = 1$ (± 0.03) which does not cause observable displacement of the beams. After generation, both the laser beam and the generated harmonics propagate through the plan-parallel crystal [Fig. 5(b)] and their propagation remain parallel after leaving the crystal. This is in confliction with the assumption that the harmonics are generated inside the crystal, represented in Fig. 2(a), but in full agreement with the measurement results. The same can be expected if the harmonics are generated on the rear surface of the crystal. The laser beam propagates through the crystal and after leaving the crystal, the harmonics are generated outside the crystal from the states of Σ_{CB} collinearly to the laser beam.

To investigate the harmonics generated on the quasi 2D layer of the Σ_{CB} states we performed the calculations presented in Fig. 4(b). In our surface computations, we assume that in the ground state, the 3 valence electrons of the Al atom are bound, so that we have a quasi Al^{3+} ion with empty 3s state. In the excited state, one electron is promoted to the 3s orbital, so that the ion becomes Al^{2+}. Accordingly, we have used the primitive (hexagonal) cell [26] to implement a 2D

OSA CONTINUUM

monolayer of Al^{2+} ions by fixing their positions in space and using mixed periodic boundary conditions for excitation in the out-of-plane direction with a grid spacing of 20 pm and $n_k = 24$ in the two periodic dimensions for obtaining converged result. The harmonic spectrum generated on the surface is fundamentally different from the bulk case of Fig. 4(c) and similar to the measurements. The 3rd and 5th harmonics are dominant, as in the measurements; they have a high contrast with low background, as in the measurements. The calculations produce some 2nd and 4th order harmonics and predict the appearance of a weak 7th harmonic, but they are below the 10^{-4} background (noise) level of the measurements and would not be visible even if they were present. Indeed, using a larger number of k-points in the simulations such as $n_k = 48$, the intensity of the background and the 2nd and 4th harmonics decrease 16-fold while the intensity of the odd harmonics remains intact. This means that the calculations shown with $n_k = 24$ are accurately converged for the 3rd and 5th harmonics and that the 2nd and 4th harmonics, if present, should be much weaker. We have tested simulations with $n_k > 48$ for a definite convergence of the 2nd and 4th harmonics but they are almost prohibitive due to computational costs. Furthermore, the polarization dependence of the even harmonics follows the 4-fold symmetry of the grid instead of the 6-fold symmetry of the atoms, hence the appearance of even harmonics are only numerical artifacts.

In Fig. 4(d), we compare the dependence of the measured (AlN layer on the front side) 3rd and 5th harmonic intensities on the polarization direction of the driving laser beam to the bulk and surface simulations. In the measurement, the polarization angle was set by using a half-wave plate. The measurements exhibit no polarization dependence of the 3rd harmonic and a small 6-fold dependence of the 5th harmonic. The polarization dependence calculated from bulk crystal however gives 6-fold dependence for both the 3rd and 5th harmonic with similar modulation depth. Significantly, the calculations from surface wave function predict almost no (or very weak) polarization dependence of 3rd harmonic and 6-fold polarization dependence of the 5th harmonic with somewhat larger modulation depth than in the experiment.

7. Conclusion

We have performed a series of experiments and calculations where all observations qualitatively and quantitatively contradict the bulk origin of the harmonic generation in solids and support a dominating surface origin. (1) we have observed collinear propagation of the 3rd and 5th harmonics with the generating laser beam. (2) we have shown that the shape of the generated harmonic spectra calculated from the surface conduction band wave function qualitatively describe the experimental observations, while calculations made by considering the bulk crystal do not. (3) The polarization dependence of the generated harmonics contrasts with the bulk origin.

Funding. European Metrology Programme for Innovation and Research (CC4C); Ministerio de Economía y Competitividad (FIS2017-85526-R); Horizon 2020 Framework Programme (856415).

Acknowledgment. The authors thank Erin Young for growing and characterizing the AlN samples.

Disclosures. The authors declare no conflicts of interest.

References

1. J. Li, J. Lu, A. Chew, S. Han, J. Li, Y. Wu, H. Wang, S. Ghimire, and Z. Chang, "Attosecond science based on high harmonic generation from gases and solids," Nat. Commun. **11**(1), 2748 (2020).
2. T. T. Luu, V. Scagnoli, S. Saha, L. J. Heyderman, and H. J. Wörner, "Generation of coherent extreme ultraviolet radiation from α–quartz using 50 fs laser pulses at a 1030 nm wavelength and high repetition rates," Opt. Lett. **43**(8), 1790–1793 (2018).
3. H. Kim, S. Han, Y. W. Kim, S. Kim, and S.-W. Kim, "Generation of Coherent Extreme-Ultraviolet Radiation from Bulk Sapphire Crystal," ACS Photonics **4**(7), 1627–1632 (2017).
4. J. Seres, E. Seres, C. Serrat, and T. Schumm, "Non-perturbative generation of DUV/VUV harmonics from crystal surfaces at 108 MHz repetition rate," Opt. Express **26**(17), 21900–21909 (2018).

OSA CONTINUUM

5. J. Seres, E. Seres, C. Serrat, E. C. Young, J. S. Speck, and T. Schumm, "All-solid-state VUV frequency comb at 160 nm using high-harmonic generation in nonlinear femtosecond enhancement cavity," Opt. Express **27**(5), 6618–6628 (2019).
6. S. Han, L. Ortmann, H. Kim, Y. W. Kim, T. Oka, A. Chacon, B. Doran, M. Ciappina, M. Lewenstein, S.-W. Kim, S. Kim, and A. S. Landsman, "Extraction of higher-order nonlinear electronic response in solids using high harmonic generation," Nat. Commun. **10**(1), 3272 (2019).
7. T. Dekorsy, R. Ott, and H. Kurz, "Bloch oscillations at room temperature," Phys. Rev. B **51**(23), 17275–17278 (1995).
8. G. Vampa, C. R. McDonald, G. Orlando, P. B. Corkum, and T. Brabec, "Semiclassical analysis of high harmonic generation in bulk crystals," Phys. Rev. B **91**(6), 064302 (2015).
9. T. T. Luu and H. J. Worner, "High-order harmonic generation in solids: A unifying approach," Phys. Rev. B **94**(11), 115164 (2016).
10. G. Le Breton, A. Rubio, and N. Tancogne-Dejean, "High-harmonic generation from few-layer hexagonal boron nitride: Evolution from monolayer to bulk response," Phys. Rev. B **98**(16), 165308 (2018).
11. G. Vampa, H. Liu, T. F. Heinz, and D. A. Reis, "Disentangling interface and bulk contributions to high-harmonic emission from solids," Optica **6**(5), 553–556 (2019).
12. T. Y. F. Tsang, "Optical third-harmonic generation at interfaces," Phys. Rev. A **52**(5), 4116–4125 (1995).
13. T. Y. F. Tsang, "Third- and fifth-harmonic generation at the interfaces of glass and liquids," Phys. Rev. A **54**(6), 5454–5457 (1996).
14. G. Yi, H. Lee, J. Jiannan, B. J. Chun, S. Han, H. Kim, Y. W. Kim, D. Kim, S.-W. Kim, and Y.-J. Kim, "Nonlinear third harmonic generation at crystalline sapphires," Opt. Express **25**(21), 26002–26010 (2017).
15. N. Yoshikawa, T. Tamaya, and K. Tanaka, "High-harmonic generation in graphene enhanced by elliptically polarized light excitation," Science **356**(6339), 736–738 (2017).
16. H. Liu, Y. Li, Y. S. You, S. Ghimire, T. F. Heinz, and D. A. Reis, "High-harmonic generation from an atomically thin semiconductor," Nat. Phys. **13**(3), 262–265 (2017).
17. Y. Gao, H. Lee, J. Jiao, B. J. Chun, S. Kim, D.-H. Kim, and Y.-J. Kim, "Surface third and fifth harmonic generation at crystalline Si for non-invasive inspection of Si wafer's inter-layer defects," Opt. Express **26**(25), 32812–32823 (2018).
18. N. Tancogne-Dejean and A. Rubio, "Atomic-like high-harmonic generation from two-dimensional materials," Sci. Adv. **4**(2), eaao5207 (2018).
19. S. Loughin, R. H. French, W. Y. Ching, Y. N. Xu, and G. A. Slack, "Electronic structure of aluminum nitride: Theory and experiment," Appl. Phys. Lett. **63**(9), 1182–1184 (1993).
20. J. Pastrnak and L. Roskovcova, "Refraction index measurements on AlN single crystals," Phys. Status Solidi B **14**(1), K5–K8 (1966).
21. D. Kecik, C. Bacaksiz, R. T. Senger, and E. Durgun, "Layer- and strain-dependent optoelectronic properties of hexagonal AlN," Phys. Rev. B **92**(16), 165408 (2015).
22. E. Kuokstis, J. Zhang, Q. Fareed, J. W. Yang, G. Simin, M. Asif Khan, R. Gaska, M. Shur, C. Rojo, and L. Schowalter, "Near-band-edge photoluminescence of wurtzite-type AlN," Appl. Phys. Lett. **81**(15), 2755–2757 (2002).
23. R. W. Boyd, *Nonlinear Optics*, 3rd ed. (Elsevier, 2008).
24. M. A. L. Marques, A. Castro, G. F. Bertsch, and A. Rubio, "Octopus: a first-principles tool for excited electron–ion dynamics," Comput. Phys. Commun. **151**(1), 60–78 (2003).
25. X. Andrade, D. Strubbe, U. De Giovannini, A. H. Larsen, M. J. Oliveira, J. Alberdi-Rodriguez, A. Varas, I. Theophilou, N. Helbig, M. J. Verstraete, L. Stella, F. Nogueira, A. Aspuru-Guzik, A. Castro, M. A. Marques, and A. Rubio, "Real-space grids and the Octopus code as tools for the development of new simulation approaches for electronic systems," Phys. Chem. Chem. Phys. **17**(47), 31371–31396 (2015).
26. A. Kobayashi, O. F. Sankey, S. M. Volz, and J. D. Dow, "Semiempirical tight-binding band structures of wurtzite semiconductors: AlN, CdS, CdSe, ZnS, and ZnO," Phys. Rev. B **28**(2), 935–945 (1983).
27. S. R. Bowman, C. G. Brown, and B. Taczak, "Optical dispersion and phase matching in gallium nitride and aluminum nitride," Opt. Mater. Express **8**(4), 1091–1099 (2018).
28. A. B. Georgescu and S. Ismail-Beigi, "Surface Piezoelectricity of (0001) Sapphire," Phys. Rev. Appl. **11**(6), 064065 (2019).